AlGaN/GaN based Multi-Metal Gated High Electron Mobility Transistor with Improved Linearity

Md. Tasnim Azad, Toiyob Hossain, Bejoy Sikder, Qingyun Xie, Mengyang Yuan, Eiji Yagyu, Koon Hoo Teo, Tomás Palacios, *Fellow, IEEE*, Nadim Chowdhury, *Member, IEEE*

***Abstract*— This work proposes a multi-metal gated architecture to improve the linearity of AlGaN/GaN high electron mobility transistor (HEMT). The general idea of this architecture is to use different gate metals along the width of the device. Through experimentally calibrated technology computer-aided design (TCAD) simulation, a selection of metals along with widths that yields the lowest value of third-order transconductance (g_{m3}) has also been estimated. Single tone large signal simulation of proposed device exhibits output-referred 1dB compression point (P_{1dB}) of 1.81 W/mm, saturation output power (P_{sat}) of 6.91 W/mm, and maximum power added efficiency (PAE) of 65%, all of which are better than simulations of standard/baseline device structures. Two-tone large signal simulation shows excellent linearity performance when biased at deep class AB showing OIP3/P_{DC} of 13.7 dB which is 6.3 dB higher and IMD3 of -45.7 dBc which is 12.9 dB lower than baseline device at $V_{DS,Q} = 28$ V, $I_{D,Q} = 73$ mA/mm. These performance matrices attest to the improved linearity performance of the proposed device compared to conventional planar AlGaN/GaN HEMT.**

***Index Terms*— 5G, Linearity, AlGaN/GaN, High Electron Mobility Transistor (HEMT), Multi-Metal Gate (MMG),**

I. Introduction

5G/6G technology is poised to deliver the next generation of mobile connectivity, internet of things (IoT) applications. This high frequency technology supports the operation of modern mobile base stations which require high power density to transmit signal over long distance. As compared to Si-based Laterally Diffused Metal-Oxide-Semiconductor (LDMOS) (1 W/mm) [1] and GaAs (0.5-1.5 W/mm) [2], [3] technology, GaN HEMTs have shown superior power density-PAE combinations of 40 W/mm-60% at 4 GHz [4], 30.6 W/mm-49.6% at 8 GHz [5], 10.5 W/mm-34% at 40 GHz [6], 5.83W/mm-38.5% at 94 GHz [7], which makes GaN HEMT an excellent candidate for the next generation of high-frequency power amplifiers. To this end, significant advancements have been achieved over the years in GaN electronics [8] from device-level breakthroughs such as MIS HEMT structure [9], N-polar HEMT [7], FinFET [10], HEMT with back barrier [11] etc.

To avoid adjacent channel interference in the crowded 5G bands, the power amplifiers used in the base stations require high linearity, which constitutes a major challenge for GaN HEMTs. Furthermore, 5G communication requires high uplink and downlink transmission rates, which necessitate the use of higher order constellations such as 256-QAM (quadrature amplitude modulation) or higher. These modulation schemes feature high peak-to-average power ratio (PAPR) and require high output power back-off (OBO) because of linearity constraints. To effectively address the linearity-efficiency trade-off, the improvement of linearity in GaN transistors is highly desired.

To this end, various efforts have been made to improve GaN transistor linearity which can be broadly divided into two categories, first, the modification of epitaxial structure e.g. PolFET [12], graded channel HEMT [13], [14], nanowire channel [15], closely-coupled channel structure [16]. The other category is improvement to the basic HEMT device architecture e.g. FinFETs [17], variable-width fins [10], transitional recessed gate [18], buried gate [19], lateral gate modulation [20] and selective-area charge implantation [21]. While experimental results indicate promising performance, many of these proposed devices require non-conventional and complex epitaxial growth and/or device structures, which would limit their monolithic integration in RF integrated circuits and their widespread adoption in the growing world of 5G amplifiers.

Transconductance (g_m) and its derivatives are key device-level DC parameters with significant implications to the power amplifier's signal non-linearity. Third-order transconductance (g_{m3}) is defined as Eq.1

This work was supported in part by Bangladesh University of Engineering and Technology, in part by Information and Communications Technology Division, Government of Bangladesh, and in part by the Air Force Office of Scientific Research (AFOSR), grant no. FA9550-22-1-0367. *(M. T. Azad and T. Hossain contributed equally to this work.)*
(Corresponding author: N. Chowdhury)

M. T. Azad, T. Hossain, B. Sikder and N. Chowdhury are with the Department of Electrical and Electronic Engineering, Bangladesh University of Engineering and Technology, Dhaka-1205, Bangladesh (e-mail: {1706139, 1706013, bejoy, nadim} @eee.buet.ac.bd)

Q. Xie, and T. Palacios are with Microsystems Technology Laboratories, Massachusetts Institute of Technology, Cambridge, MA 02139, U.S.A. (e-mail: {qyxie, tpalacios} @mit.edu)

M. Yuan was with Microsystems Technology Laboratories, Massachusetts Institute of Technology, Cambridge, MA 02139, U.S.A. He is presently with Apple Inc., Cupertino, CA 95014, U.S.A. (e-mail: myyuan@alum.mit.edu)

Eiji Yagyu is with Mitsubishi Electric Corporation, Advanced Technology R&D Center, 8-1-1, Tsukaguchi-honmachi, Amagasaki City 661-8661, Japan. (e-mail: yagyu.eiji@cb.mitsubishielectric.co.jp)

K. H. Teo is with Mitsubishi Electric Research Labs, Cambridge, MA 02139, U.S.A. (e-mail: teo@merl.com)

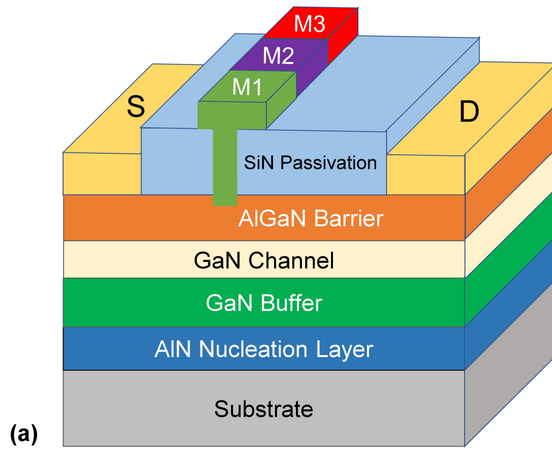

(b)

Parameters	Value
Gate Length [μm]	Foot = 0.16, Head = 0.70
Barrier Layer Thickness [nm]	21
Al Mole Fraction	0.25
Stem Height of Gate [μm]	0.21
Gate Recess [nm]	10
Gate-Drain Spacing [μm]	1.8
Gate-Source Spacing [μm]	0.85

Fig. 1. (a) 3D schematic of the proposed multi-metal gated AlGaN/GaN HEMT with optimized g_{m3} characteristics. (b) Structural parameters of the proposed device.

$$g_{m3} = \frac{d^3 I_{DS}}{dV_{GS}^3} \tag{1}$$

This work proposes a novel multi-metal gated (MMG) HEMT structure with improved linearity. A gate structure with different metal work functions along the gate width is proposed to optimize g_{m3} profile. Up to 10 different metals are studied to optimize linearity. As compared to earlier reported devices of higher linearity, highlights of the proposed device include: the device is based on a conventional AlGaN/GaN epitaxial structure, and the planar device architecture has been preserved, making it easier to integrate this device into complex RF front-ends in the future. More importantly, this work offers improved linearity in deep AB zone where the majority of the high-efficiency power amplifiers (PAs) (e.g. mobile handsets, 5G base stations) operate. A simple optimization technique is proposed to help choose the metal structures that maximize linearity.

The organization of the article is as follows. Section II presents device structure and simulation methodology. Section III describes the results and discussion from device level to circuit level and analyzes the origin of improvement of linearity. Finally, Section IV concludes the article.

II. Device Structure and Simulation Methodology

Fig. 1(a) shows a 3D schematic of the proposed multi-metal gated (MMG) AlGaN/GaN HEMT. An undoped AlGaN barrier has a thickness of 21 nm with a gate recess of 10 nm. The source-gate distance (L_{GS}) and the source-drain distance (L_{SD}) of the device are 0.85 μm and 2.81 μm respectively. Other important structural parameters are listed in Fig. 1(b). The MMG HEMT's channel and source/drain access regions are identical to the conventional planar HEMT. The gate of the MMG HEMT is composed of different metals for threshold voltage variation. Due to differences in the processing conditions of various gate metal deposition steps, the interface of gate metal of the MMG HEMT would likely be different than planar HEMT. At the same time, the MMG HEMT employs the same gate recess depth for each of the gate metal regions. To simplify the schematic, 3 metals (M_1–M_3) have been shown in Fig. 1(a) but the number of metals and width of each metal heavily influence the peak of third-order transconductance (g_{m3}) and hence is subjected to optimization as will be discussed later.

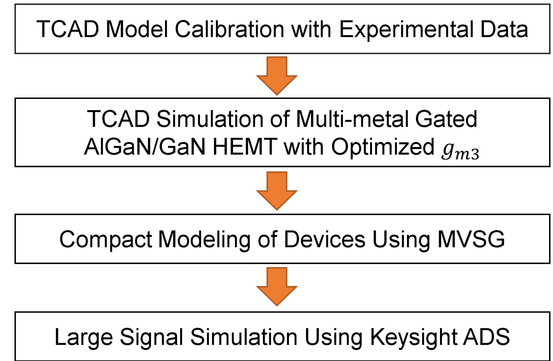

Fig. 2. Methodology of this study. The methodology follows TCAD model calibration, TCAD simulation, compact modeling, and large signal circuit simulation, in chronological order.

The methodology adopted for this work is shown in Fig. 2. To calibrate the models (mobility, charge etc.) in Silvaco TCAD [22], experimental data [23] of a planar AlGaN/GaN HEMT has been matched. Exactly the same epitaxial structure was used as [23] to calibrate the TCAD model. An excellent fit is obtained between TCAD simulation and experimental data, as illustrated in the output characteristics [Fig. 3(a)] and transfer characteristics (including the sub-threshold region) 3(b)]. Subsequently, the proposed multi-metal gated HEMT is simulated using the same model parameters (obtained from the fitting) as shown in Fig. 3(c). The drain to source length (L_{SD}) and gate to drain length (L_{GD}) were modified for the purpose of the work to typical RF HEMTs suitable for operation at $V_{DS,Q} = 28$ V.

Then, an optimization algorithm is used to select the metals and their corresponding widths that minimize g_{m3}. In order to estimate the large signal RF performance, compact modeling of both proposed device and planar HEMT was performed using the MIT Virtual Source GaN-HEMT (MVSG) model [24]. Single tone and two-tone large-signal simulations have been conducted in Keysight ADS [25] to estimate the linearity performance matrices of both devices.

III. Results and Discussion

A. TCAD Simulation

After obtaining an excellent fit between TCAD simulations and experimental data, the I_D-V_{GS} and I_D-V_{DS} characteristics for 10 different metals (Ta, Ti, Cr, Ag, Ru, W, Au, Ni, Ir,

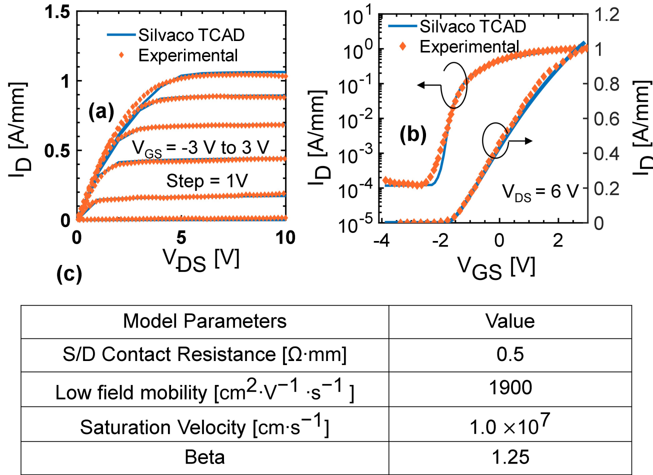

Model Parameters	Value
S/D Contact Resistance [Ω·mm]	0.5
Low field mobility [$cm^2 \cdot V^{-1} \cdot s^{-1}$]	1900
Saturation Velocity [$cm \cdot s^{-1}$]	1.0×10^7
Beta	1.25

Fig. 3. Calibration of TCAD simulation models based on experimental data taken from [23] (a) I_D-V_{DS} (b) I_D-V_{GS} characteristics. (c) Simulation parameters of the calibrated models.

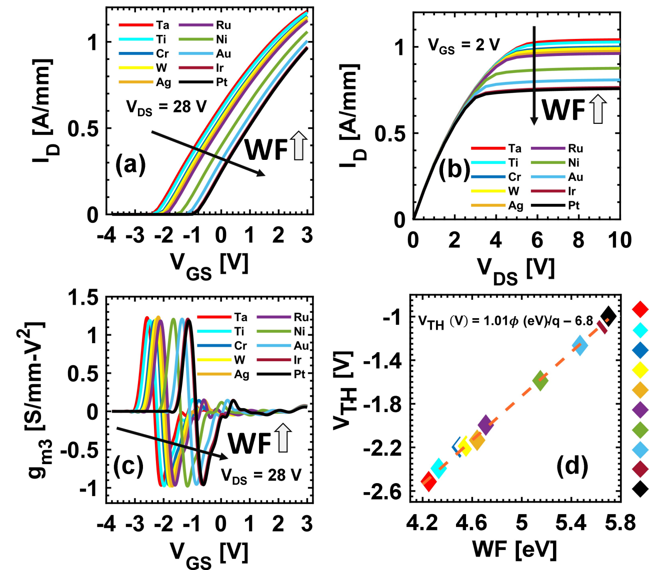

Fig. 4. (a) Simulated I_D-V_{GS} (b) I_D-V_{DS} and (c) g_{m3} *vs.* V_{GS} characteristics of a recessed gated AlGaN/GaN HEMT with different gate metals. (d) Dependence of threshold voltage on the work-function of gate metal of AlGaN/GaN HEMT. The dependence is shown as a linear equation.

Pt) have been simulated as shown in Fig. 4(a)–(b). Ten metals with ten different work-functions ranging from 4.25 eV – 5.70 eV [26], [27] were chosen for this study. Gate work-function modulates the threshold voltage of the HEMT and the I_D-V_{GS} curve gets right-shifted in V_{GS} axis with the increase of work-function as depicted in Fig. 4(a). Fig. 4(b) shows that the saturation current decreases with an increase in work-function. As the gate metal varies, so does the associated work function of the metal, resulting in a shift in the threshold voltage, as illustrated in Fig. 4(d). This shift in threshold voltage eventually causes a distribution of different metals' g_{m3} curves across the V_{GS} axis. In Fig. 4(c) , g_{m3} profile peaks have a range of 1.52 V in the V_{GS} axis, due to work-function variation of the metals. It should be noted that, g_{m3} peak value (normalized) remained the same for devices of individual metals. The dependence of the threshold voltage on the work-function of gate metal of AlGaN/GaN HEMT can be modeled by a linear equation $V_{TH}[\mathrm{V}] = 1.01\Phi[\mathrm{eV}]/q - 6.8$, where q is the charge of an electron. The rate of change of threshold voltage with respect to work-function is 1.01 V/eV. This value is in good agreement with the experimental finding that has been reported [28]. As a proof-of-concept study, this work does not take into account the Fermi-level pinning effect which is highly dependent on the sample preparation and fabrication. Fermi level pinning factors of 0.81, 0.43 [29] and 0.71 [30] are reported, and would cause deviations in the slope of the existing linear relationship between V_{TH} and Φ as if $S = 1$ (absence of Fermi-level pinning effect). If Fermi level pinning is considered, the g_{m3} profiles would have different positions due to a change in threshold voltage. Nevertheless, the linear relationship between V_{TH} and Φ is preserved, therefore maintaining the validity of the proposed optimization algorithm for g_{m3}.

A slower turn-on of the transistor (near $V_{GS} \approx V_{TH}$, which corresponds to the quiescent bias point in deep AB operation) is highly desired to improve the linearity of highly efficient deep AB amplifiers [29]. The turn-on of the channel is dependent on charge accumulation in the AlGaN/GaN channel. Placing different metals as the gate material along the width of the device would result in different V_{TH} values in different regions of the device. The net effect is a slow turn-on as a result of slower charge accumulation, which would lower the g_{m3} of the proposed device at $V_{GS} \approx V_{TH}$.

B. g_{m3} Optimization

The proposed device is based on the superposition of parallel connected GaN HEMTs [30] with slightly different threshold voltages as demonstrated in Fig. 5(a). Different gate metals $M_1, M_2, ..., M_N$ result in transistors of distinct threshold voltages $V_{T1}, V_{T2}, ..., V_{TN}$. The choice of metals and their respective gate widths (referred as sub-gates from now on) are the goals of optimization.

While optimizing g_{m3} this work ensures the intersection of I_D-V_{GS} characteristics of conventional planar HEMT and MMG HEMT at class deep AB region so that both devices can be biased at the same gate voltage and drain current in order to compare their linearities.

The following algorithm was used to produce the best result for a combination of 6 metals. The metals excluding Ni can be divided into 2 categories. One category contains metals having work-function less than Ni and the other category contains the opposite. Fig. 5(b) shows the superposition of g_{m3} for Ni- and Ag-gated transistors, where Ag has a lower work-function than Ni and hence a lower V_{TH}. This creates a V_{GS} window (-2.0 V to -1.4 V) where g_{m3} is lowered. On the other hand, Fig. 5(c) shows the g_{m3} superposition of Ni and Ir, where Ir has a higher work-function than Ni and hence a higher V_{TH}. This also creates a V_{GS} window (-1.4 V to -1.0 V) of lower g_{m3}. Concurrent superposition of g_{m3} of Ni with g_{m3} of Ir and Ag without any optimization on their relative sub-gate widths broadens the V_{GS} window which is shown in Fig. 5(d). Fig. 5(b)–(d) shows how the superposition of g_{m3} of the sub-gates with optimized weight (sub-gate widths in this case) can

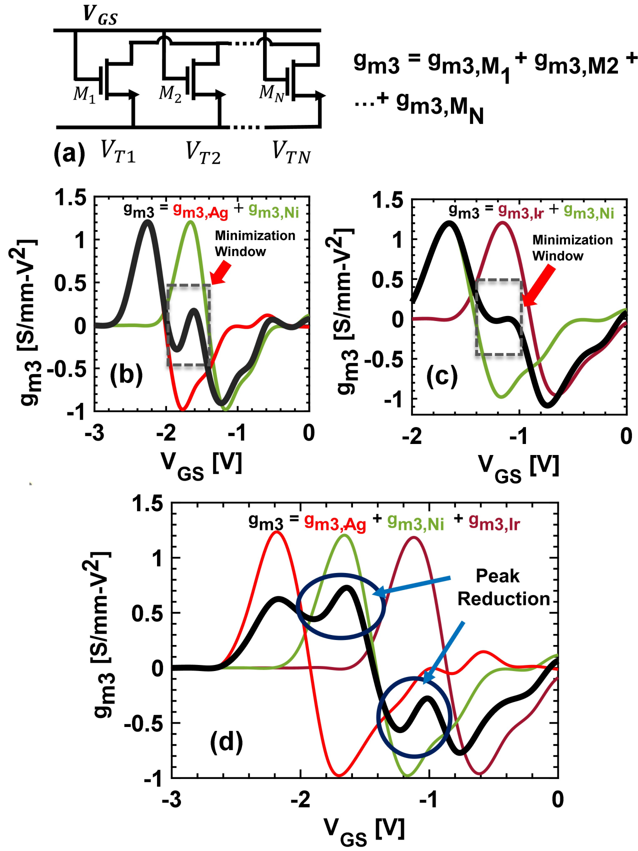

Fig. 5. (a) Multi-metal gated AlGaN/GaN HEMT acts like transistors with different gate metals connected in parallel. g_{m3} of the proposed device will be an additive superposition of individual sub-gate's ($M_1, M_2, ..M_N$) g_{m3} (b) Superposition of $g_{m3,Ni}$ and $g_{m3,Ag}$ at V_{DS} = 28 V creating a minimization window from −2.0 V to −1.4 V (where Ag has a lower Φ than Ni) (c) Superposition of $g_{m3,Ni}$ and $g_{m3,Ir}$ at V_{DS} = 28 V creating a minimization window from −1.4 V to −1.0 V (where Ir has a higher Φ than Ni) (d) A broader minimization window was achieved through superposition of $g_{m3,Ag}$, $g_{m3,Ni}$ and $g_{m3,Ir}$.

generate a composite device having very low value of g_{m3} over a broad gate-bias range.

Consequently, in this work, the widths of the sub-gates having lower and higher work-function than Ni are design parameters to improve overall device linearity. Different sub-gate structures will induce a positive and a negative peak of g_{m3} at different gate voltages. Ni was chosen for the reference V_{TH}, and its vicinity as the window to reduce g_{m3}. Superposition of g_{m3} of sub-gates weighted by their respective widths formulates the optimization equation in Fig. 5(a). The nonlinear least squares method was used to get the optimized sub-gate widths with minimal g_{m3}.

The proposed MMG HEMT turns on slowly with V_{GS} compared to conventional planar HEMT as shown in Fig. 6(a), in particular around the intersection point of the I_D-V_{GS} curves ($V_{GS} = -1.12$ V, $I_D = 73$ mA/mm). The off-state current of the MMG HEMT is impacted due to use of low work-function metal sub-gates. However, the breakdown voltage remains unaltered, as shown in Fig.6(b). Since, transconductance is the rate of change of drain current with gate voltage, and the highest rate of change of drain current is in the vicinity of threshold voltage; a lower g_m peak is a direct result of slower turn on as shown in Fig. 6(c). The algorithm used in

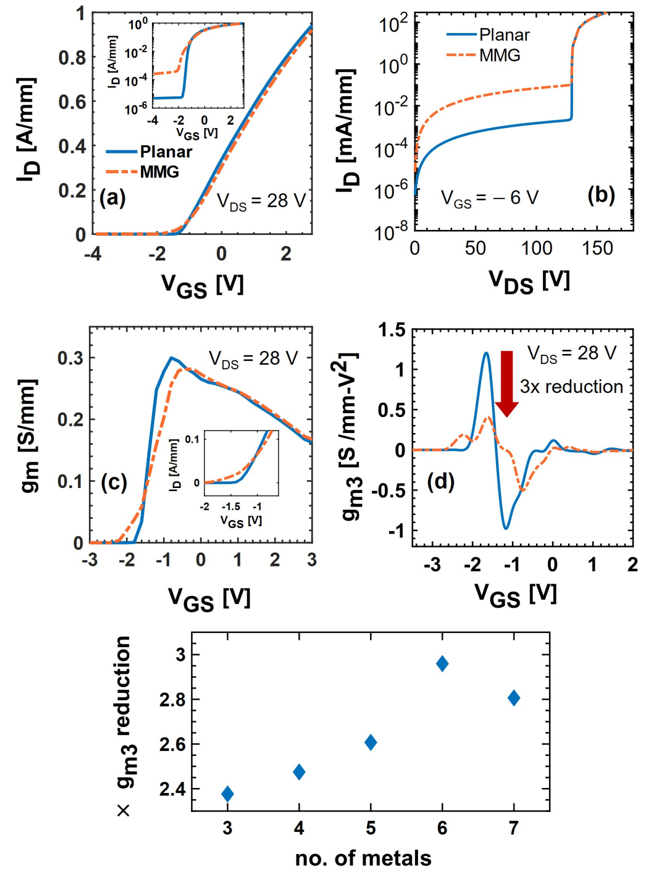

Fig. 6. Comparison of (a) I_D-V_{GS} (b) Off-state breakdown voltage, BV_{off} (c) g_m-V_{GS} and (d) g_{m3}-V_{GS} characteristics of conventional planar AlGaN/GaN HEMT and proposed Multi-metal gated AlGaN/GaN HEMT with an optimized selection of metals (W-10.53 %, Ag-5.26 %, Ni-42.11 %, Au-10.53 %, Ir-15.79 %, Pt-15.79 %) as percentage of the device width.The inset of (a) shows the semi-logarithmic I_D-V_{GS} for MMG and planar HEMT. The inset of (c) zooms into I_D-V_{GS} at $V_{GS} \approx V_{TH}$ and illustrates the slower turn-on achieved by the proposed MMG HEMT.(e) Dependence of g_{m3} peak reduction on number of metals.

this work results in 3 times reduction in g_{m3} peak for the proposed MMG HEMT in comparison to the conventional planar HEMT as shown in Fig. 6(d). An analysis is also shown in Fig. 6(e) which focuses on the selection of optimum number of metals for g_{m3} peak reduction. The optimization improves until the number of metals increases beyond 6. After that, g_{m3} deteriorates. This is because when the number of metals increases beyond 6, the positive and negative peaks of g_{m3} of some metals are too far away from the useful gate bias to have a meaningful effect on the reduction of g_{m3} of Ni.

C. Compact Modeling

To estimate the circuit-level RF performance of the devices, compact modeling of the new transistor structure and planar HEMT structure is needed. This work uses the MVSG model [24]. To obtain a good fit between the device characteristics and compact modeling, various parameters have been tuned as shown in Table I. Fig. 7(a)–(b) shows excellent matching of I_D-V_{GS} and I_D-V_{DS}. The following parameters have the highest weight when matching the I-V curves: threshold voltage

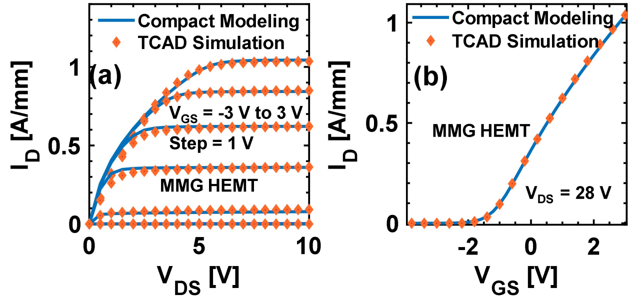

Fig. 7. (a) I_D-V_{GS} and (b) I_D-V_{DS} characteristics of proposed device exhibiting the accuracy of the compact model with respect to TCAD simulation [24].

TABLE I. MVSG Model Parameters

Parameter	MMG HEMT
C_g [nF·cm^{-2}]	455
R_{sh} [Ω/□]	300
μ_0 [cm^2·V^{-1}·s^{-1}]	1650
delta1	0
betard	0.80
betars	0.74
delta1rd	2.0
delta1rs	2.0

(V_{TH}), access region sheet resistance (R_{sh}), DIBL for drain access transistor (delta1rd), DIBL for source access transistor (delta1rs), gate areal capacitance (C_g), subthreshold slope (S), drain access areal capacitance (C_{grs}), low field mobility (μ_0), DIBL (delta1), linear to saturation transition parameters (betard, betars).

D. Large Signal Simulation

The planar model is a conventional Ni gated AlGaN/GaN HEMT and the proposed HEMT is a multi-metal gated architecture with optimized width of the chosen metals. After tuning load and source impedances for optimum PAE, single-tone large signal simulation of the proposed and conventional AlGaN/GaN HEMT was performed at a frequency of 5 GHz while biased at deep class AB. In the simulation, $V_{DS,Q} = 28$ V, $V_{GS,Q} = -1.12$ V ($I_{D,Q} = 73$ mA/mm), and the total gate width of each device is 100 μm.

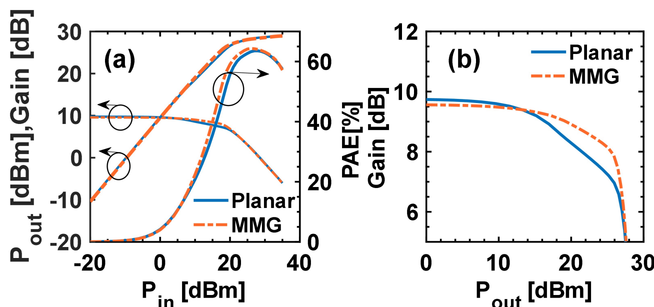

Fig. 8. Single tone large signal simulation of the proposed and conventional AlGaN/GaN HEMT biased at class AB with V_{DS} = 28 V , V_{GS} = −1.12 V, $I_{D,Q}$ = 73 mA/mm and f = 5 GHz.

Fig. 8(a) shows that the maximum PAE of the MMG HEMT obtained is 65% and P_{sat} is 28.4 dBm. The soft compression on AlGaN/GaN HEMT is delayed in the case of the MMG HEMT. Fig. 8(b) shows that 1 dB compression point of the MMG HEMT is at 22.58 dBm output power, while it is at 17.78 dBm for the planar HEMT which indicates nearly 5 dB advantage in the output power in case of operating at 1 dB compression point.

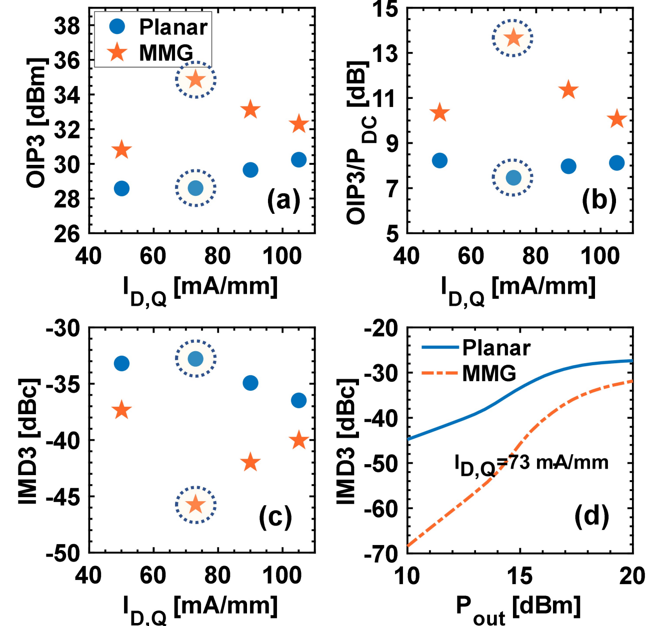

Fig. 9. Two-tone load-pull results for conventional planar HEMT and proposed MMG HEMT at different current bias (a) OIP3 (b) OIP3/P_{DC} (c) IMD3 at different $I_{D,Q}$, (d) IMD3 at different output powers for conventional planar HEMT and MMG HEMT. The sweet spot at $I_{D,Q}$=73 mA/mm, where MMG HEMT has the best performance compared to conventional HEMT is circled in (a),(b), and (c).

TABLE II. Summary of the performance metrics of the planar HEMT and the MMG HEMT.

Parameter	Planar HEMT	MMG HEMT
Width [μm]	100	100
$V_{DS,Q}$ [V]	28	28
f_T [GHz]	131	123
f_{max} [GHz]	213	203
$V_{GS,Q}$ [V]	−1.12	−1.12
$I_{D,Q}$ [mA/mm]	73	73
Γ_L	$0.86\angle 2.88°$	$0.86\angle 2.88°$
Γ_S	$0.88\angle -33.6°$	$0.88\angle -33.6°$
Linear Gain [dB]	9.75	9.56
Max. PAE [%]	63.55	65.00
P_{sat} [W/mm]	7.00	6.91
P_{1dB} [W/mm]	0.595	1.81
OIP3/P_{DC} [dB]	7.40	13.7
IMD3 [dBc]	−32.8	−45.7

For the two-tone load-pull setup, center frequency was chosen at 5 GHz with a frequency spacing of 10 MHz. Both conventional HEMT and MMG HEMT were biased at $V_{DS} = 28$ V and $I_{D,Q} = \{50, 73, 90, 105\}$ mA/mm. All four bias points belong to the deep class AB region of operation. For a fair comparison between two devices on large signal linearity, the performance metrics were compared at a particular output power (P_{out}). This article reports a sweet spot for the linearity specifications while comparing the two devices. Among the four quiescent bias points, at 73 mA/mm, the gate bias

TABLE III. Benchmarking of device-level load-pull and linearity figure of merits.

Reference	Platform	Transistor Type	Frequency (GHz)	P_{out} (W/mm)	PAE (%)	OIP3 (dBm)	OIP3/P_{DC} (dB)
[10] MIT 2017	AlGaN/GaN	Variable Width Fin-HEMT	6	1.90	–	36	20
[12] OSU 2019	Graded AlGaN/GaN	PolFET w/ LPCVD-SiN_x	10	3.40	40	39	13.30
[31] UCSB 2020	GaN/AlGaN (N-polar)	N-polar GaN MIS-HEMT	30	0.30	17	32	15.00
[32] NGC 2020	AlGaN/GaN Superlattice	SLC FET	30	9.50	41	36	14.00
[19] Bilkent 2021	AlGaN/GaN	Buried Gate	3.5	–	–	31.7	–
[16] HKUST 2021	AlGaN/AlN/GaN/AlN/GaN	Closely Coupled Double-Channel Structure	4	1.62	43	33.9	–
[33] UCAS 2022	AlGaN/GaN	HEMT w/ LPCVD-SiN_x	1	0.20	19	28.1	4.36
[34] HRL 2022	AlGaN/Graded-AlGaN /GaN/AlGaN	Graded Channel HEMT	30	–	–	36	17.50
[21] Xidian 2022	AlGaN/GaN	HEMT w/ selective-area charge implantation	12	6.70	47	39.2	11.20
[35] Xidian 2023	AlGaN/GaN/Graded-AlGaN:Si-doped/GaN	Double Channel HEMT	3.6	0.75	58	39.3	10.10
This Work [Simulation]	**AlGaN/GaN**	**MMG HEMT**	**5**	**6.91**	**65**	**34.9**	**13.70**

($V_{GS,Q} = -1.12$ V) is same for both devices. At $I_{D,Q} = 73$ mA/mm, OIP3 for the planar device is 28.6 dBm, and 34.86 dBm for MMG HEMT, leaving a 6.26 dB improvement (Fig. 9(a)). At the same bias, OIP3/P_{DC} is 7.46 dB for planar HEMT and 13.66 dB for the MMG HEMT, a 6.2 dB improvement as depicted in Fig. 9(b). Fig. 9(c) shows a comparision between two devices in terms of IMD3. At the reported sweet spot, the planar HEMT has an IMD3 of −32.8 dBc whereas the proposed MMG HEMT has an IMD3 of −45.7 dBc.

Table II summarizes the important figure of merits of the transistors analyzed in this work. In the MMG HEMT, the slight reduction in f_T and f_{max} is mainly due to the drop in maximum transconductance value. OIP3/P_{DC} and IMD3 in Table II have been reported at $P_{out} = 15$ dBm. In Fig. 9(d), IMD3 of the two devices are compared for a range of output power while biased at $I_{D,Q} = 73$ mA/mm. The MMG HEMT shows significantly improved IMD3 than the conventional HEMT over a considerable range of output power (10 –20 dBm).

It is confirmed that, the device-level reduction on g_{m3} at the bias point has resulted in better large-signal RF linearity performance. Table III shows a comparison among high linear AlGaN/GaN HEMT in recent years and MMG HEMT in terms of linearity figure of merits. MMG HEMT can ensure excellent linearity with high PAE and P_{out} values.

IV. Conclusion

This work proposes a multi-metal gated AlGaN/GaN HEMT structure that achieves enhancement in linearity and high power efficiency, which are both extremely important for 5G communication. The proposed device exhibits 1 dB compression point of 22.6 dBm which is nearly 5 dB higher than the conventional planar HEMT. Two-tone simulation result shows that the proposed device shows an OIP3/P_{DC} of 13.7 dB whereas that of the conventional planar HEMT is 7.4 dB while biased at deep AB. These results highlight the improvement in linearity and also show the high prospect of proposed multi-metal gated AlGaN/GaN HEMT structure in the next generation mobile communication.

References

[1] S. Theeuwen, H. Mollee, R. Heeres, and F. Van Rijs, "LDMOS Technology for Power Amplifiers Up to 12 GHz," in *2018 13th European Microwave Integrated Circuits Conference (EuMIC)*. IEEE, 2018. doi: 10.23919/EuMIC.2018.8539904 pp. 162–165.

[2] K.-S. Kong, B. Nguyen, S. Nayak, and M.-Y. Kao, "Ka-Band MMIC High Power Amplifier (4W at 30GHz) with Record Compact Size," in *IEEE Compound Semiconductor Integrated Circuit Symposium, 2005. CSIC'05*. IEEE, 2005. doi: 10.1109/CSICS.2005.1531822 pp. 4–pp.

[3] C. F. Campbell, D. C. Dumka, M.-Y. Kao, and D. M. Fanning, "High Efficiency Ka-band Power Amplifier MMIC Utilizing a High Voltage Dual Field Plate GaAs PHEMT Process," in *2011 IEEE Compound Semiconductor Integrated Circuit Symposium (CSICS)*. IEEE, 2011. doi: 10.1109/CSICS.2011.6062436 pp. 1–4.

[4] Y.-F. Wu, M. Moore, A. Saxler, T. Wisleder, and P. Parikh, "40-W/mm Double Field-plated GaN HEMTs," in *2006 64th Device Research Conference*. IEEE, 2006. doi: 10.1109/DRC.2006.305162 pp. 151–152.

[5] Y.-F. Wu, A. Saxler, M. Moore, R. Smith, S. Sheppard, P. Chavarkar, T. Wisleder, U. Mishra, and P. Parikh, "30-W/mm GaN HEMTs by Field Plate Optimization," *IEEE Electron Device Letters*, vol. 25, no. 3, pp. 117–119, 2004. doi: 10.1109/LED.2003.822667

[6] T. Palacios, A. Chakraborty, S. Rajan, C. Poblenz, S. Keller, S. DenBaars, J. Speck, and U. Mishra, "High-Power AlGaN/GaN HEMTs for Ka-Band Applications," *IEEE Electron Device Letters*, vol. 26, no. 11, pp. 781–783, 2005. doi: 10.1109/LED.2005.857701

[7] W. Li, B. Romanczyk, M. Guidry, E. Akso, N. Hatui, C. Wurm, W. Liu, P. Shrestha, H. Collins, C. Clymore, S. Keller, and U. K. Mishra, "Record RF Power Performance at 94 GHz From Millimeter-Wave N-Polar GaN-on-Sapphire Deep-Recess HEMTs," *IEEE Transactions on Electron Devices*, pp. 1–6, 2023. doi: 10.1109/TED.2023.3240683

[8] K. H. Teo, Y. Zhang, N. Chowdhury, S. Rakheja, R. Ma, Q. Xie, E. Yagyu, K. Yamanaka, K. Li, and T. Palacios, "Emerging GaN technologies for power, RF, digital, and quantum computing applications: Recent advances and prospects," *Journal of Applied Physics*, vol. 130, no. 16, p. 160902, October 2021. doi: 10.1063/5.0061555

[9] H. W. Then, M. Radosavljevic, P. Koirala, M. Beumer, S. Bader, A. Zubair, T. Hoff, R. Jordan, T. Michaelos, J. Peck *et al.*, "Scaled submicron field-plated enhancement mode high-K Gallium Nitride transistors on 300mm Si(111) wafer with power FoM ($r_{ON} \times q_{GG}$)

of 3.1 mohm-nC at 40V and f_t/f_{MAX} of 130/680ghz," in *2022 International Electron Devices Meeting (IEDM)*. IEEE, 2022. doi: 10.1109/IEDM45625.2022.10019373 pp. 35.1.1–35.1.4.

[10] S. Joglekar, U. Radhakrishna, D. Piedra, D. Antoniadis, and T. Palacios, "Large Signal Linearity Enhancement of AlGaN/GaN High Electron Mobility Transistors by Device-level V_T Engineering for Transconductance Compensation," in *2017 IEEE International Electron Devices Meeting (IEDM)*. IEEE, 2017. doi: 10.1109/IEDM.2017.8268457 pp. 25–3.

[11] D. S. Lee, X. Gao, S. Guo, D. Kopp, P. Fay, and T. Palacios, "300-GHz InAlN/GaN HEMTs With InGaN Back Barrier," *IEEE Electron Device Letters*, vol. 32, no. 11, pp. 1525–1527, 2011. doi: 10.1109/LED.2011.2164613

[12] S. H. Sohel, M. W. Rahman, A. Xie, E. Beam, Y. Cui, M. Kruzich, H. Xue, T. Razzak, S. Bajaj, Y. Cao *et al.*, "Linearity Improvement with AlGaN Polarization- Graded Field Effect Transistors with Low Pressure Chemical Vapor Deposition Grown SiN_x Passivation," *IEEE Electron Device Letters*, vol. 41, no. 1, pp. 19–22, 2019. doi: 10.1109/LED.2019.2951655

[13] J. Chang, S. Afroz, K. Nagamatsu, K. Frey, S. Saluru, J. Merkel, S. Taylor, E. Stewart, S. Gupta, and R. Howell, "The Super-Lattice Castellated Field-Effect Transistor: A High-Power, High-Performance RF Amplifier," *IEEE Electron Device Letters*, vol. 40, no. 7, pp. 1048–1051, 2019. doi: 10.1109/LED.2019.2917285

[14] Q. Yu, C. Shi, L. Yang, H. Lu, M. Zhang, M. Wu, B. Hou, F. Jia, F. Guo, X. Ma, and Y. Hao, "High Current and Linearity AlGaN/GaN/-Graded-AlGaN:Si-doped/GaN Heterostructure for Low Voltage Power Amplifier Application," *IEEE Electron Device Letters*, pp. 1–1, 2023. doi: 10.1109/LED.2023.3241763

[15] D. S. Lee, H. Wang, A. Hsu, M. Azize, O. Laboutin, Y. Cao, J. W. Johnson, E. Beam, A. Ketterson, M. L. Schuette *et al.*, "Nanowire Channel InAlN/GaN HEMTs With High Linearity of g_m and f_T," *IEEE Electron Device Letters*, vol. 34, no. 8, pp. 969–971, 2013. doi: 10.1109/LED.2013.2261913

[16] W. Song, Z. Zheng, T. Chen, J. Wei, L. Yuan, and K. J. Chen, "Rf linearity enhancement of gan-on-si hemts with a closely coupled double-channel structure," *IEEE Electron Device Letters*, vol. 42, no. 8, pp. 1116–1119, 2021. doi: 10.1109/LED.2021.3087785

[17] K. Zhang, Y. Kong, G. Zhu, J. Zhou, X. Yu, C. Kong, Z. Li, and T. Chen, "High-Linearity AlGaN/GaN FinFETs for Microwave Power Applications," *IEEE Electron Device Letters*, vol. 38, no. 5, pp. 615–618, 2017. doi: 10.1109/LED.2017.2687440

[18] S. Wu, X. Ma, L. Yang, M. Mi, M. Zhang, M. Wu, Y. Lu, H. Zhang, C. Yi, and Y. Hao, "A Millimeter-Wave AlGaN/GaN HEMT Fabricated With Transitional-Recessed-Gate Technology for High-Gain and High-Linearity Applications," *IEEE Electron Device Letters*, vol. 40, no. 6, pp. 846–849, 2019. doi: 10.1109/LED.2019.2909770

[19] O. Odabaşı, D. Yılmaz, E. Aras, K. E. Asan, S. Zafar, B. Ç. Akoğlu, B. Bütün, and E. Özbay, "AlGaN/GaN-Based Laterally Gated High-Electron-Mobility Transistors With Optimized Linearity," *IEEE Transactions on Electron Devices*, vol. 68, no. 3, pp. 1016–1023, 2021. doi: 10.1109/TED.2021.3053221

[20] K. Shinohara, C. King, A. D. Carter, E. J. Regan, A. Arias, J. Bergman, M. Urteaga, and B. Brar, "GaN-Based Field-Effect Transistors With Laterally Gated Two-Dimensional Electron Gas," *IEEE Electron Device Letters*, vol. 39, no. 3, pp. 417–420, 2018. doi: 10.1109/LED.2018.2797940

[21] F. Zhang, X. Zheng, H. Zhang, M. Mi, Y. He, M. Du, X. Ma, and Y. Hao, "Linearity Enhancement of AlGaN/GaN HEMTs With Selective-Area Charge Implantation," *IEEE Electron Device Letters*, vol. 43, no. 11, pp. 1838–1841, Nov 2022. doi: 10.1109/LED.2022.3208121

[22] Silvaco, "Silvaco ATLAS manual," 2023.

[23] Y. Zhang, K. Wei, S. Huang, X. Wang, Y. Zheng, G. Liu, X. Chen, Y. Li, and X. Liu, "High-Temperature-Recessed Millimeter-Wave AlGaN/GaN HEMTs With 42.8% Power-Added-Efficiency at 35 GHz," *IEEE Electron Device Letters*, vol. 39, no. 5, pp. 727–730, 2018. doi: 10.1109/LED.2018.2822259

[24] U. Radhakrishna, P. Choi, and D. A. Antoniadis, "Facilitation of GaN-Based RF- and HV-Circuit Designs Using MVS-GaN HEMT Compact Model," *IEEE Transactions on Electron Devices*, vol. 66, no. 1, pp. 95–105, Jan 2019. doi: 10.1109/TED.2018.2848721

[25] Keysight, "Advanced Design System (ADS) manual," 2023.

[26] H. B. Michaelson, "The work function of the elements and its periodicity," *Journal of Applied Physics*, vol. 48, no. 11, pp. 4729–4733, 1977. doi: 10.1063/1.323539

[27] B. Ofuonye, J. Lee, M. Yan, C. Sun, J.-M. Zuo, and I. Adesida, "Electrical and microstructural properties of thermally annealed Ni/Au and Ni/Pt/Au Schottky contacts on AlGaN/GaN heterostructures," *Semiconductor Science and Technology*, vol. 29, no. 9, p. 095005, 2014. doi: 10.1088/0268-1242/29/9/095005

[28] G. Li, T. Zimmermann, Y. Cao, C. Lian, X. Xing, R. Wang, P. Fay, H. G. Xing, and D. Jena, "Threshold Voltage Control in $Al_{0.72}Ga_{0.28}N$/AlN/GaN HEMTs by Work-Function Engineering," *IEEE Electron Device Letters*, vol. 31, no. 9, pp. 954–956, 2010. doi: 10.1109/LED.2010.2052912

[29] H. Lu, B. Hou, L. Yang, X. Niu, Z. Si, M. Zhang, M. Wu, M. Mi, Q. Zhu, K. Cheng *et al.*, "AlN/GaN/InGaN Coupling-Channel HEMTs for Improved g_m and Gain Linearity," *IEEE Transactions on Electron Devices*, vol. 68, no. 7, pp. 3308–3313, 2021. doi: 10.1109/TED.2021.3082104

[30] R. P. Martinez, D. J. Munzer, B. Shankar, B. Murmann, and S. Chowdhury, "Linearity Performance of Derivative Superposition in GaN HEMTs: A Device-to-Circuit Perspective," *IEEE Transactions on Electron Devices*, 2023. doi: 10.1109/TED.2023.3259383

[31] P. Shrestha, M. Guidry, B. Romanczyk, N. Hatui, C. Wurm, A. Krishna, S. S. Pasayat, R. R. Karnaty, S. Keller, J. F. Buckwalter *et al.*, "High Linearity and High Gain Performance of N-polar GaN MIS-HEMT at 30 GHz," *IEEE Electron Device Letters*, vol. 41, no. 5, pp. 681–684, 2020. doi: 10.1109/LED.2020.2980841

[32] J. Chang, S. Afroz, B. Novak, J. Merkel, K. Nagamatsu, and R. Howell, "Advances in the Super-Lattice Castellated Field Effect Transistor (SLCFET) for High Power Density, Energy Efficient RF Amplification," in *2020 IEEE/MTT-S International Microwave Symposium (IMS)*, 2020. doi: 10.1109/IMS30576.2020.9224099 pp. 576–579.

[33] G. Jing, X. Wang, S. Huang, Q. Jiang, K. Deng, Y. Wang, Y. Li, J. Fan, K. Wei, and X. Liu, "Mechanism of Linearity Improvement in GaN HEMTs by Low Pressure Chemical Vapor Deposition-SiNx Passivation," *IEEE Transactions on Electron Devices*, vol. 69, no. 12, pp. 6610–6615, 2022. doi: 10.1109/TED.2022.3213636

[34] J.-S. Moon, B. Grabar, J. Wong, J. Tai, E. Arkun, D. V. Morales, C. Dao, S. Bharadwaj, D. Fanning, N. Venkatesan *et al.*, "Highly Linear and Efficient mm-Wave GaN HEMTs and MMICs," in *2022 IEEE/MTT-S International Microwave Symposium-IMS 2022*. IEEE, 2022. doi: 10.1109/IMS37962.2022.9865424 pp. 302–304.

[35] Q. Yu, C. Shi, L. Yang, H. Lu, M. Zhang, M. Wu, B. Hou, F. Jia, F. Guo, X. Ma, and Y. Hao, "High Current and Linearity AlGaN/GaN/-Graded-AlGaN:Si-doped/GaN Heterostructure for Low Voltage Power Amplifier Application," *IEEE Electron Device Letters*, vol. 44, no. 4, pp. 582–585, 2023. doi: 10.1109/LED.2023.3241763